Polarization Imaging Descattering Based on Dark Channel Prior Background Light Estimation

Jiarui Zhang , Yaxin Cai, and Ming Fang

Abstract—In turbid water environments, conventional polarimetric imaging descattering methods usually rely on selecting a non-target background region as a substitute for global background light information, leading to image clarity. By integrating polarization imaging with the dark channel prior (DCP) and fully utilizing the polarization information from the Stokes vector and the DCP, the interference of the target information in calculating the background information can be effectively eliminated. This method also enables accurate estimation of the global distribution for the degree of polarization (DoP) and the angle of polarization (AoP) of the backscattered light and eliminates the need for the complex process of background region selection. Experimental results with varying turbid water concentrations demonstrate the proposed method's effectiveness for target recovery in both underwater images with and without background regions. Compared with the conventional active polarization imaging model, our method improves image contrast by 47% in the strongly scattering environment.

Index Terms—Active polarization imaging, background light estimation, dark channel prior, descattering.

I. INTRODUCTION

UNDERWATER optical imaging is extensively emplo-yed in seabed resource exploration, underwater rescue operations, and environmental monitoring [1]. How-ever, the interaction of light with suspended particles in water causes scattering and absorption, which degrade imaging quality. Absorption reduces light intensity, while scattering introduces backscattered light, which is superimposed on the light reflected from the target. This superposition obscures the target, significantly lowering imaging contrast [2].

To improve the quality of underwater images, researchers have proposed several techniques, including distance picking [3], image fusion [4], dark channel prior (DCP) [5], Constrained Contrast Adaptive Histogram Equalization (CLAHE) [6], and deep learning methods [7], [8], [9]. Polarization imaging has become an effective method for suppressing backscattered light to obtain clear underwater images due to its simple system structure and significant improvement in imaging clarity. Schechner derived the transmission process of polarized light in water to establish the passive underwater polarization imaging model [10]. Following this, Huang et al. considered the polarization characteristics of the target and solved the estimation of the degree of polarization (DoP) of the target [11]. Amer et al. proposed an improved DCP method based on a low-pass polarization filter [12]. Hu et al. integrated an imaging model with a neural network to optimize polarization parameters [8], [13]. Numerous experimental results have demonstrated the effectiveness of these methods. However, since these approaches rely on natural light conditions, they are less effective in deep water. Treibitz et al. employed polarized illumination to establish the underwater active polarization imaging model, effectively separating background and target information [14]. This approach further enhances imaging contrast and clarity through active polarization imaging. Dubreuil introduced optical correlation into polarization imaging [15]. Zhao et al. applied a genetic algorithm to simultaneously estimate the DoP of both target light and backscattered light, achieving a significant descattering effect without prior information [16]. However, this method overlooks the fact that the polarization characteristics of backscattered light vary with spatial position, leading to some errors in fitting the backscattered polarization information in the target region. Hu et al. estimated the spatial distribution of the DoP and the intensity of backscattered light using interpolation and least squares, significantly improving the quality of underwater images [17]. However, this method requires manual selection of the background region, which impedes real-time detection and processing. Wang et al. automatically recovered a clear image of the images without background region by estimating the parameters of the backscattered light through an intermediate variable [18]. However, this method is based on the assumption of omitting the DoP of directly reflected light from the target. There are difficulties in dealing with targets other than fully depolarized [19], [20], [21].

Aiming at the above problems, this paper proposes a background-independent descattering method combining polari-zation and DCP, which enhances underwater imaging by fully utilizing the polarization information, including DoP and AoP of the Stokes vector. By exploiting the differences in polarization characteristics between the backscattered light in the target and background regions to recover an explicit scene even in the absence of the background region. It achieves this by

acquiring a dark channel image, which effectively prevents interference from the target signal when computing background light, and then accurately estimates the global distributions of AoP and DoP of the backscattered light. Experimental results demonstrate that the method effectively eliminates back-scattered light while preserving the intensity information of the target, allowing for the target image to be well recovered regardless of the images with or without the background region.

II. THEORY AND METHOD

A. Underwater Active Polarization Imaging Model

Based on the traditional polarization imaging recovery model, the total light intensity received by the detector can be divided into two components, assuming that forward scattering, which causes image blurring, is negligible. One component is the direct reflected light from the target, i.e., the target signal light. The other component is the backscattered light from the scattering medium, i.e., the background light. The total light intensity I can thus be expressed as

$$I = T + B, \qquad (1)$$

where T represents the target light intensity, and B denotes the backscattered light intensity. Based on the polarization imaging method, the detector front polarizer is adjusted to be parallel or perpendicular to the polarization state of the backscattered light. This allows for the acquisition of two images ($I_\parallel$ and $I_\perp$), which correspond to the maximum and minimum visible backscattering, respectively. These images are expressed as

$$\begin{cases} I_\parallel = T_\parallel + B_\parallel \\ I_\perp = T_\perp + B_\perp \end{cases}, \qquad (2)$$

$$I_\parallel + I_\perp = T + B = I, \qquad (3)$$

where the subscripts $\parallel$ and $\perp$ denote the relationship (parallel or perpendicular) between the polarization state of the polarizer and the polarization state of the backscattered light, respectively. In addition, the DoP of target light and backscattered light can be expressed as

$$\begin{cases} P_T = \frac{T_\parallel - T_\perp}{T_\parallel + T_\perp} \\ P_B = \frac{B_\parallel - B_\perp}{B_\parallel + B_\perp} \end{cases}, \qquad (4)$$

where P_T is the DoP of the target light and P_B is the DoP of backscattered light.

From (1)–(4), the expressions for the target light (T) and backscattered light (B) are given as

$$T = \frac{[I_\perp(1 + P_B) - I_\parallel(1 - P_B)]}{P_B - P_T}, \qquad (5)$$

$$B = \frac{[I_\parallel(1 - P_T) - I_\perp(1 + P_T)]}{P_B - P_T}. \qquad (6)$$

By obtaining four key parameters ($I_\parallel$, $I_\perp$, P_B and P_T), a clear underwater scene can be recovered from a degraded image using (5) and (6). According to (5), P_T only acts as a scaling factor for the brightness of the restored result. Thus, according to the papers [14], [22], P_T is treated as a constant across the entire scene. Since manually rotating the polarization detector

is time-consuming and prone to visual observation errors, Deng et al. [23] proposed generating the optimal image pairs directly using the Stokes vector. Therefore, obtaining accurate AoP distribution of the backscattered light and P_B distribution is the key to rebuilding the target. However, because the target and backscattered light are superimposed in the target region and exhibit different polarization characteristics, the AoP and P_B distributions cannot typically be computed independently [22]. Thus, removing the interference from the target information is crucial for accurately calculating the background information.

B. Removal of Target Information Based on DCP

He et al. first proposed the definition of the DCP, which states that in most localized regions of an image, excluding the sky, some pixels typically have very low intensity in at least one colour channel [5]. If J is an outdoor image without haze, the intensity of J^{dark} is low and tends to 0, except in sky regions. Therefore, J^{dark} is called the dark channel image, and this statistical observation is known as DCP. J^{dark} can be represented as

$$J^{dark} = \min_{y \in \Omega(x)} \left(\min_{c \in \{r,g,b\}} J^c(y) \right), \qquad (7)$$

where J^c denotes each channel of the image and $\Omega(x)$ is a local region centered at x.

After the introduction of DCP, Drews et al. applied it to underwater image recovery to remove scattered light [24]. Guan et al. proposed an improved dehazing method that combines DCP with an underwater polarization imaging model [25]. This method leverages the polarization characteristics of light to enhance the efficiency and accuracy of target detection in scattering environments. However, target and background information are always superimposed in the image, which hinders the accurate estimation of the polarization characteristics of backscattered light. Due to scattering caused by haze particles, pixel intensities in the dark channel do not converge to 0 in degraded underwater images, as these intensities are primarily influenced by scattered light. Drawing from DCP, the target light typically exhibits at least one channel with the lowest intensity. For grayscale images, according to (1), there is always a region where $T = 0$. Minimizing the grayscale image allows the point where $T = 0$ can be identified, allowing the total light intensity to converge to the backscattered intensity, i.e., I is infinitely close to B. This effectively removes the target information from the image.

C. Estimation AoP of Backscattered Light Based on DCP

Active linear polarized light is used to illuminate the underwater scene, with the Stokes vector serving as the input image. In this case, the only difference in the polarization characteristics of the light source is the direction of polarization. The Stokes vector S consists of four elements and is expressed in the following form

$$S = \begin{bmatrix} I \\ Q \\ U \\ V \end{bmatrix} = \begin{bmatrix} I_0(x,y) + I_{90}(x,y) \\ I_0(x,y) - I_{90}(x,y) \\ I_{45}(x,y) - I_{135}(x,y) \\ I_r(x,y) - I_l(x,y) \end{bmatrix}, \qquad (8)$$

where $I_0(x, y)$, $I_{45}(x, y)$, $I_{90}(x, y)$, $I_{135}(x, y)$ denote the polarized light intensity at the polarization angles of 0°, 45°, 90°, and 135° respectively, and V denotes the circularly polarized component, $I_r(x, y)$ denotes the right-handed circularly-polarized light intensity, $I_l(x, y)$ denotes the left-handed circularly polarized light intensity. Circular polarization accounts for only a small fraction of light and can be neglected, i.e., $V = 0$ [23]. The AoP of the polarized light written as θ_B is calculated as

$$\theta_B(x, y) = \frac{1}{2} \arctan \frac{U(x, y)}{Q(x, y)}, \tag{9}$$

When polarized light illuminates targets other than fully depolarized targets, the Q and U images inevitably contain target-related information. This contamination leads to inaccuracies in calculating θ_B, the angle of backscattered light by particles in water. To resolve this issue, this paper proposes a method to remove target signals from the Q and U images based on DCP, allowing for a more accurate estimation of the global θ_B.

According to (7), the dark channel images Q^{dark} and U^{dark} of Q and U can be calculated as

$$Q^{dark} = \min_{y \in \Omega(x)} \left(\min_{c \in \{r,g,b\}} Q^c(y) \right), \tag{10}$$

$$U^{dark} = \min_{y \in \Omega(x)} \left(\min_{c \in \{r,g,b\}} U^c(y) \right). \tag{11}$$

Thereby, the exact AoP of the backscattered light named as $\overset{\wedge}{\theta}_B$ can be computed as

$$\overset{\wedge}{\theta}_B(x, y) = \frac{1}{2} \arctan \frac{U^{dark}(x, y)}{Q^{dark}(x, y)}. \tag{12}$$

When the angle is set equal to or 90° from the $\overset{\wedge}{\theta}_B$ [23], then $I_{\parallel}$ and $I_{\perp}$ are obtained directly by

$$I_{\parallel} = \frac{1}{2} \left(I + Q \cos 2\overset{\wedge}{\theta}_B + U \sin 2\overset{\wedge}{\theta}_B \right), \tag{13}$$

$$I_{\perp} = \frac{1}{2} \left[I + Q \cos 2 \left(\overset{\wedge}{\theta}_B + \frac{\pi}{2} \right) + U \sin 2 \left(\overset{\wedge}{\theta}_B + \frac{\pi}{2} \right) \right]. \tag{14}$$

D. Global Estimation of P_B Based on DCP

In existing polarization imaging studies, P_B is commonly assumed to be uniform, with a single value estimated for P_B [14], [16]. However, there are differences in the optical paths of the backscattered light in the target and background regions, with the optical path in the target region being shorter and less scattering occurring, resulting in different intensity and polarization characteristics of the backscattered light in the target and background regions. Additionally, illumination with actively polarized light induces light field non-uniformity, which causes the backscattered light to be nonuniform as well [23], [26]. Due to these factors, estimating the DoP of the target region based on the background region introduces errors [27]. Moreover, the conventional method fails when the background region is too small or inaccurately selected. Since P_B is essential for eliminating backscattered light, accurately estimating
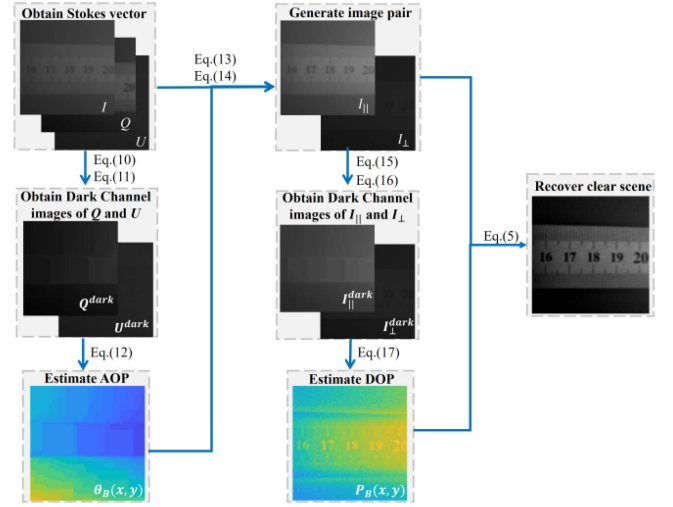

Fig. 1. Flowchart of polarization imaging descattering based on DCP background light estimation.

its spatial variation is necessary for fully automated image recovery and to expand the practical applications of underwater polarization imaging techniques. To achieve this, the proposed method removes the target interference in the backscattered light calculation using dark channel processing, thereby enabling a global estimation of the intensity and polarization characteristics of the backscattered light.

According to (2) and (3), if we ignore the polarization characteristics of the target and regard $I_{\parallel}$ and $I_{\perp}$ images as $B_{\parallel}$ and $B_{\perp}$, we can obtain the target information $T = 0$, which is obviously incorrect. For a highly polarized target, $I_{\parallel}$ and $I_{\perp}$ images will contain target information that interferes with the calculation of backscattered light. To address this issue, this paper utilizes DCP again to extract the dark channel images of $I_{\parallel}$ and $I_{\perp}$, effectively removing target information and enabling the accurate global estimation of backscattered light.

Based on (7), (13) and (14), the dark channel images of $I_{\parallel}$ and $I_{\perp}$ are computed respectively as

$$I_{\parallel}^{dark} = \min_{y \in \Omega(x)} \left(\min_{c \in \{r,g,b\}} I_{\parallel}^c(y) \right), \tag{15}$$

$$I_{\perp}^{dark} = \min_{y \in \Omega(x)} \left(\min_{c \in \{r,g,b\}} I_{\perp}^c(y) \right). \tag{16}$$

Combined with (4), the global distribution of P_B can be accurately estimated

$$P_B(x, y) = \frac{B_{\parallel} - B_{\perp}}{B_{\parallel} + B_{\perp}} = \frac{I_{\parallel}^{dark} - I_{\perp}^{dark}}{I_{\parallel}^{dark} + I_{\perp}^{dark}}. \tag{17}$$

A high-contrast and clear scene image can be obtained by substituting the accurately estimated global backscattered light polarization into (5). The overall algorithm flowchart is illustrated in Fig. 1.
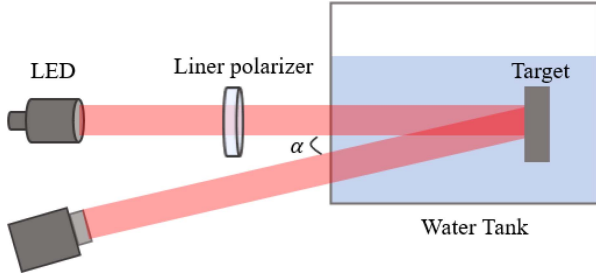
Fig. 2. Experimental setup for underwater imaging.

Fig. 3. Intensity image of steel ruler in clear water.

III. EXPERIMENT

The experimental setup for underwater polarization imaging is illustrated in Fig. 2. Scattering is influenced by the wavelength of the active illumination, with red light undergoing fewer scattering events than other wavelengths of visible light at the same detection distance. Additionally, the scattering coefficient decreases as the wavelength increases within the visible range [27]. An LED (Thorlabs M625L4-C1) with a central wavelength of 625 nm is selected as the illumination source to achieve better suppression of scattering. The light emitted by the LED passes through a polarization state generator (PSG), producing linearly polarized light and traversing the water column to the target surface. A polariza-tion camera (Daheng Imaging MER2-503-36U3 M POL) was used to capture four images at different polarization angles (0°, 45°, 90°, and 135°). Since the camera and the light source cannot be positioned exactly at the same location, the angle between them can be set within the range of [15°, 40°], as discussed in the literature [26], [28], [29]. In this study, we set the angle between the camera and the light source (α) to 30°, which primarily affects the scene's brightness. During actual image capture, adjusting the exposure time effectively ensures that the image brightness stays within the appropriate range. The light source and the polarization camera are on the same side of a transparent glass water tank (100 cm × 40 cm × 35 cm). The inner wall of the water tank was covered with black light absorbing paper to minimize the effect of reflected light from the surface of the water tank on the experimental results.

50 L of water is added to the tank, followed by skimmed milk to simulate particle scattering. The choice of skim milk as the turbid solute is motivated by its widespread use in modeling turbid seawater environments in research within this field [15], [23]. Skimmed milk primarily contains biological protein particles ranging (0.04–0.3 μm), which are comparable to suspended particles in seawater that cause significant backscattering [21], [30], [31]. According to Mie scattering theory, the scattering coefficient is influenced by particle size and scatterer concentration under independent scattering conditions. The scattering coefficient μ_s of skimmed milk is 0.42 c/cm, where c represents the milk concentration in water [12], [32]. Thus, the scattering effect can be adjusted by controlling the volume of milk added. Initially, 100 mL of skimmed milk was added, yielding a milk concentration of 2.056 g/L, and images were captured. The volume of skimmed milk was gradually
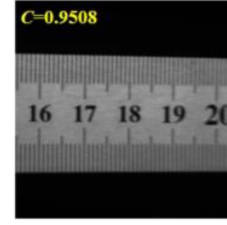
increased, with corresponding images acquired at each step, until a final volume of 200 mL was reached, resulting in a milk concentration of 4.104 g/L. The milk concentrations for 100 mL, 120 mL, 140 mL, 160 mL, 180 mL, and 200 mL are 2.056 g/L, 2.466 g/L, 2.876 g/L, 3.285 g/L, 3.695 g/L, and 4.104 g/L, respectively. Image contrast (C) [10], [16], structural similarity (SSIM) [33] and the value of the measure of enhancement (EME) [11] were selected to evaluate the image recovery effect. These metrics may be expressed separately as

$$C = \frac{\sqrt{\frac{1}{N}\sum_{x,y}^{N}\left[I(x,y)-\widetilde{I}\right]^2}}{\widetilde{I}}, \tag{18}$$

where N is the number of pixels in the image, $\tilde{I}$ is the average gray value of the pixels in the entire image, and $I(x, y)$ denotes the gray value of the pixel located at (x, y).

$$SSIM = \frac{(2\mu_x\mu_y + C_1)(2\sigma_{xy} + C_2)}{(\mu_x^2 + \mu_y^2 + C_1)(\sigma_x^2 + \sigma_y^2 + C_2)}, \tag{19}$$

where μ_x, μ_y are the mean of image (x, y) and σ_x, σ_y are the covariance of image (x, y).

$$EME = \left|\frac{1}{k_1 k_2}\sum_{l=1}^{k_2}\sum_{k=1}^{k_1} 20\log\frac{i^\omega_{\max;k,l}(x,y)}{i^\omega_{\min;k,l}(x,y)+q}\right|, \tag{20}$$

where the image is split up into $k_1 \times k_2$ blocks with the sequence number of (k, l) at two dimensions, while $i^w_{\max;k,l}(x, y)$ and $i^w_{\min;k,l}(x, y)$ are the maximum and minimum values in the blocks ω with sequence number of (k, l) in the image, and q (equals to 0.0001) is a small constant to avoid being divided by zero without considerably modifying the result of EME. For the three-evaluation metrics, the larger the value of C, the more dispersed the grayscale values of the image, and the clearer the image appears. The closer the SSlM is to 1, the greater the similarity between the two images, with the recovery image resembling the clear water image without scattering media. A higher EME value signifies better image quality. Steel rulers with high polarization are used as targets in media with varying concentrations. The steel rulers, which feature large flat surfaces as well as fine details such as tick marks, are well-suited for validating the effectiveness of different imaging methods. Fig. 3 shows the image of the target in clear water, with its C value noted in the upper left corner.
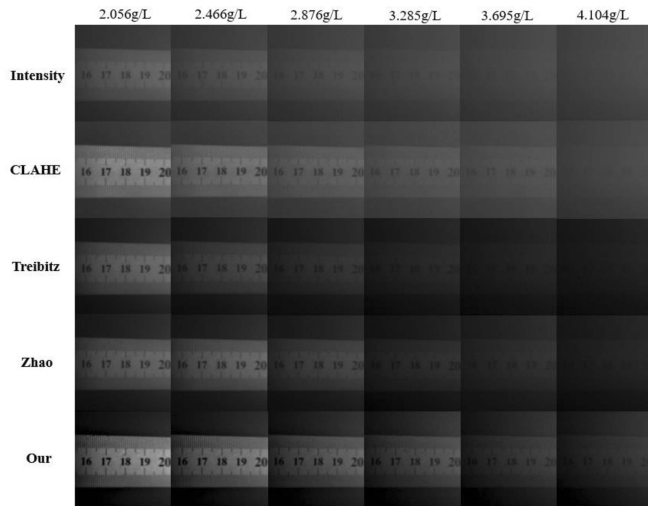
Fig. 4. Recovery results of steel rulers between the proposed method and the others in different milk concentrations.

Fig. 5. Comparison of the C between the proposed method and the others at different milk concentrations.

IV. RESULTS AND DISCUSSION

A. Scattering Suppression Effect of the Images With Background Region

To verify the robustness and effectiveness of the proposed method, images taken in water with different media concentrations are restored. Fig. 4 presents the results of the CLAHE [6], the method of Treibitz [14], the method of Zhao [16] and the proposed method for recovering steel ruler images with background regions. CLAHE is a digital image processing technique derived from histogram equalization. The traditional underwater active polarization imaging method, i.e., the Treibitz method, assumes that the P_B is uniformly and stably distributed across the entire imaging region, and the P_B is obtained by manually intercepting a patch of non-targeted background region and calculating the mean value. Zhao's method uses the genetic algorithm to automatically estimate the DoP of the target light and the backscattered light.

Scattering medium concentration refers to the number of particles per unit volume. Under the same conditions, the higher the medium concentration, the higher the probability of collision with medium particles during transmission through the medium, the corresponding scattering coefficient also increases. The effect of milk concentration on the quality of underwater polarization imaging is primarily reflected in its impact on light scattering. As the milk concentration increases, the backscattering coefficient of particles in the water also rises, causing the light to scatter multiple times before reaching the target. This generates more backscattered noise, which obscures the target.

As shown in the second row of Fig. 4, while the CLAHE enhances image contrast, it fails to address the haze caused by scattered particles effectively. As shown in the third and fourth rows of Fig. 4, the methods of Treibitz and Zhao produce recovered images that are similar to the proposed method when the milk concentration is 2.056 g/L. However, this similarity quickly diminishes as the milk concentration increases. These methods treat the background information as constant and cannot remove
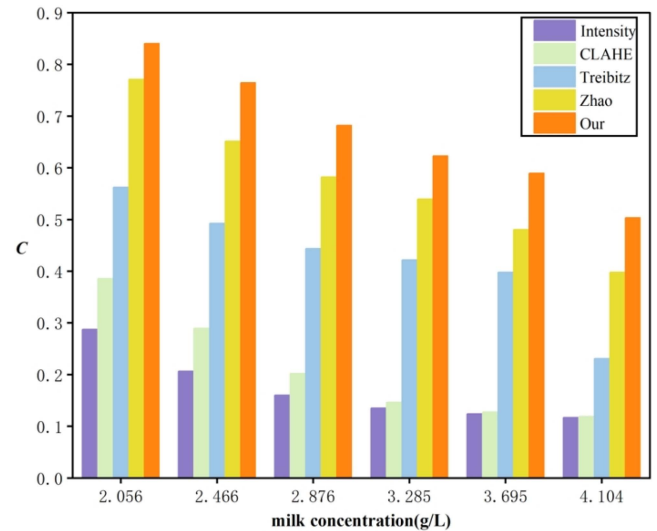
TABLE I
C OF RECOVERED IMAGES BY DIFFERENT METHODS IN FIG. 4

Milk concentration	Contrast(C)				
	Intensity	CLAHE	Treibitz	Zhao	Our
2.056g/L	0.2873	0.3858	0.5626	0.7709	**0.8403**
2.466g/L	0.2063	0.2893	0.4925	0.6517	**0.7645**
2.876g/L	0.1601	0.2019	0.4437	0.5823	**0.6820**
3.285g/L	0.1352	0.1464	0.4219	0.5396	**0.6228**
3.695g/L	0.1239	0.1278	0.3980	0.4802	**0.5895**
4.104g/L	0.1167	0.1191	0.2312	0.3982	**0.5034**

backscattered light at high concentrations. Consequently, in areas where the scale value of the steel ruler should result in a pixel value of 0. The residual haze introduces high gray values, leading to unclear targets in the recovered images.

In contrast, as shown in the fifth row of Fig. 4, the proposed method accurately calculates the global P_B distribution by eliminating target information interference through DCP. This results in a uniform illumination distribution and superior descattering performance. Even as the milk concentration increases, the proposed method achieves high-definition recovery of the edge of the numerals and scale edges of the steel ruler. Note that the intensity images arise from the target with high DoP, for which most recovery methods are ineffective.

The C values of the recovered images for each method are shown in Fig. 5 and Table I, while the evaluation results for SSIM and EME at different concentrations are summarized in Figs. 6 and 7, respectively. Compared to the directly captured intensity images, the proposed method produced significantly higher evaluation values and achieved the best performance at all milk concentrations. In particular, at the low milk concentration of 2.056 g/L, the proposed method was close to the image contrast values in clear water. The second-best method produced results very similar to those of the proposed method, demonstrating that other methods can also effectively improve image quality at
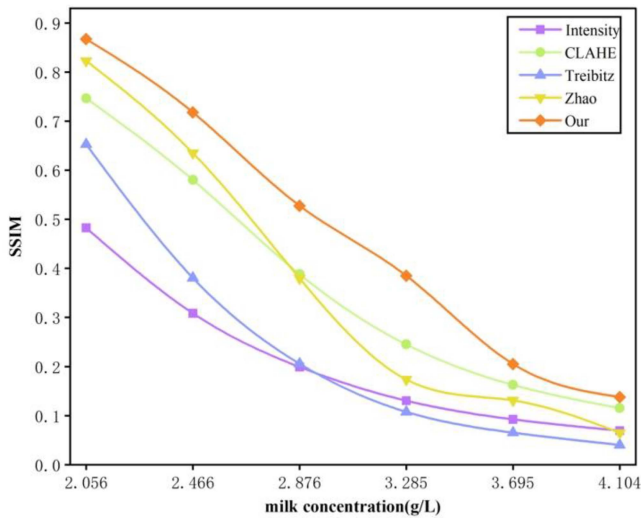
Fig. 6. Comparison of the SSIM between the proposed method and the others at different milk concentrations.
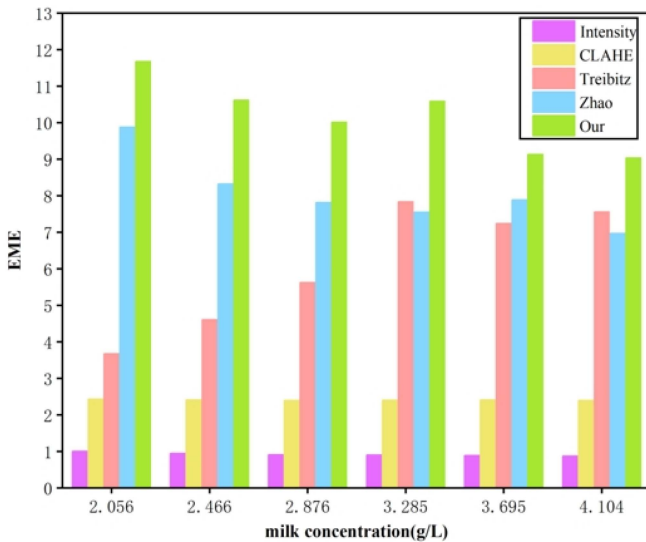

Fig. 7. Comparison of the EME between the proposed method and the others at different milk concentrations.

low concentrations. However, the advantages of the proposed method become more pronounced as the milk concentration increases. For example, in a strongly scattering environment with a milk concentration of 3.695 g/L, the proposed method improves contrast by approximately 47% compared to Treibitz's conventional active polarization imaging method.

The grayscale histogram represents the distribution of gray levels in an image. It provides a frequency count of all pixels according to their gray values. This distribution reflects the overall appearance and quality of the image, playing a crucial role in image enhancement processes. Fig. 8 illustrates the histograms of images recovered by different methods with 2.056 g/L and 4.104 g/L milk concentrations in the scattering medium. The horizontal and vertical coordinates denote the gray level and the number of pixels, respectively.

In Fig. 8(a), the histogram of the intensity image ranges from 30 to 110, while CLAHE stretches the range to 20–150, enhancing image contrast. The method of Treibitz shifts the gray value distribution to a lower range, with the gray values of background region mainly concentrated between 10 and 40. Compared with the method of Zhao histograms ranging from 1–130, the proposed method extends the gray value distribution from 0 to 180, with most background region pixels having a value of 0, while the target region displays bright scale lines and values. This indicates complete suppression of backscattered light throughout the region.

In the milk concentration of 4.104 g/L case (Fig. 8(b)), the gray value histogram of the intensity image narrows significantly, reducing the effect of CLAHE compared to the milk concentration of 2.056 g/L case. The histograms for the methods of Treibitz and Zhao show offset peaks and further narrowing, implying that the recovered images contain less information and that image details are submerged. This aligns with the visual observation of image darkening. In contrast, the histogram range of the target image from the proposed method is doubled, with a more uniform distribution and a distinct boundary between the target and background, demonstrating its effectiveness in improving image visualiz-ation in high-concentration turbid water.

B. Scattering Suppression Effect of the Images Without Background Region

To verify the scattering suppression effect of the proposed method for the images without background region. The original intensity images acquired at milk concentrations of 2.466 g/L and 3.695 g/L were cropped to remove the background region, resulting in intensity images without the background (shown in the first columns of Fig. 9(a) and (b), respectively). Since the Treibitz method requires the background region for image recovery, the results of the proposed method will be compared only with those obtained by the CLAHE method and the method proposed by Zhao in the comparison experiments of this sub-section.

As shown in Fig. 9(a), for the recovery results at the milk concentration of 2.466 g/L, some target information, such as scale lines of the steel ruler are partially lost in the intensity imaging. Although the images recovered by the method of Zhao and the proposed method appear "darker", the images recovered using CLAHE suffer from nonuniform brightness, and the haze remains unremoved. In Fig. 9(b), although the effectiveness of the method of Zhao is better than the CLAHE method for milk concentration of 3.695 g/L, a comparison shows that the images of the proposed method have better subjective visibility. The intensity distribution curves along the blue line in Fig. 9(c) and (d) for both concentrations show that the proposed method exhibits the strongest curve fluctuations, with more 0-pixel points compared to other methods. It indicates that the proposed method is not constrained by the image background region. A superior scattering suppression effect is achieved in images without background region, significantly improving image visibility and information retention.
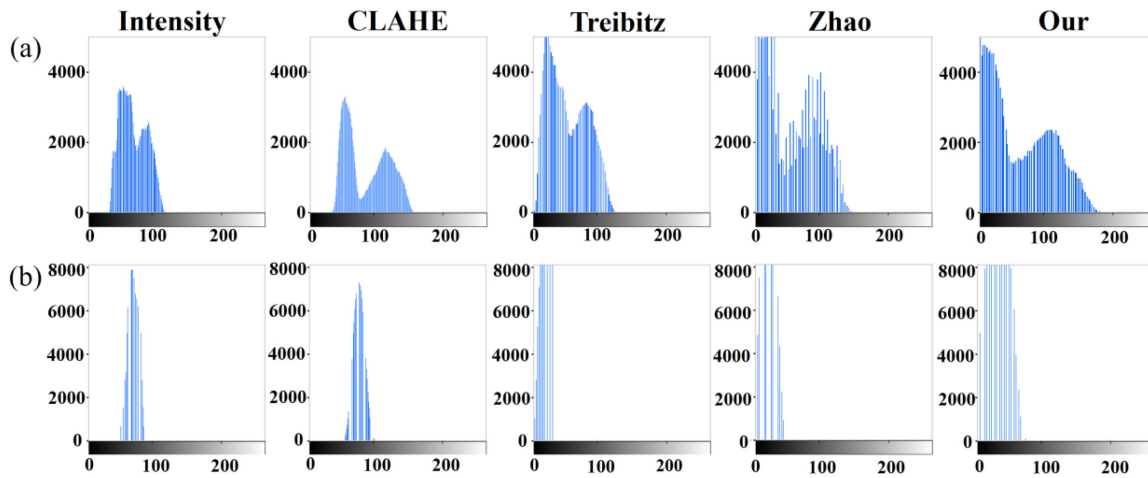
Fig. 8. (a) Histogram distribution of the recovery results (the first column of Fig. 4) of different methods for images with background region in milk concentration of 2.056 g/L. (b) Histogram distribution of the recovery results (the last column of Fig. 4) of different methods for images with background region in milk concentration of 4.104 g/L.
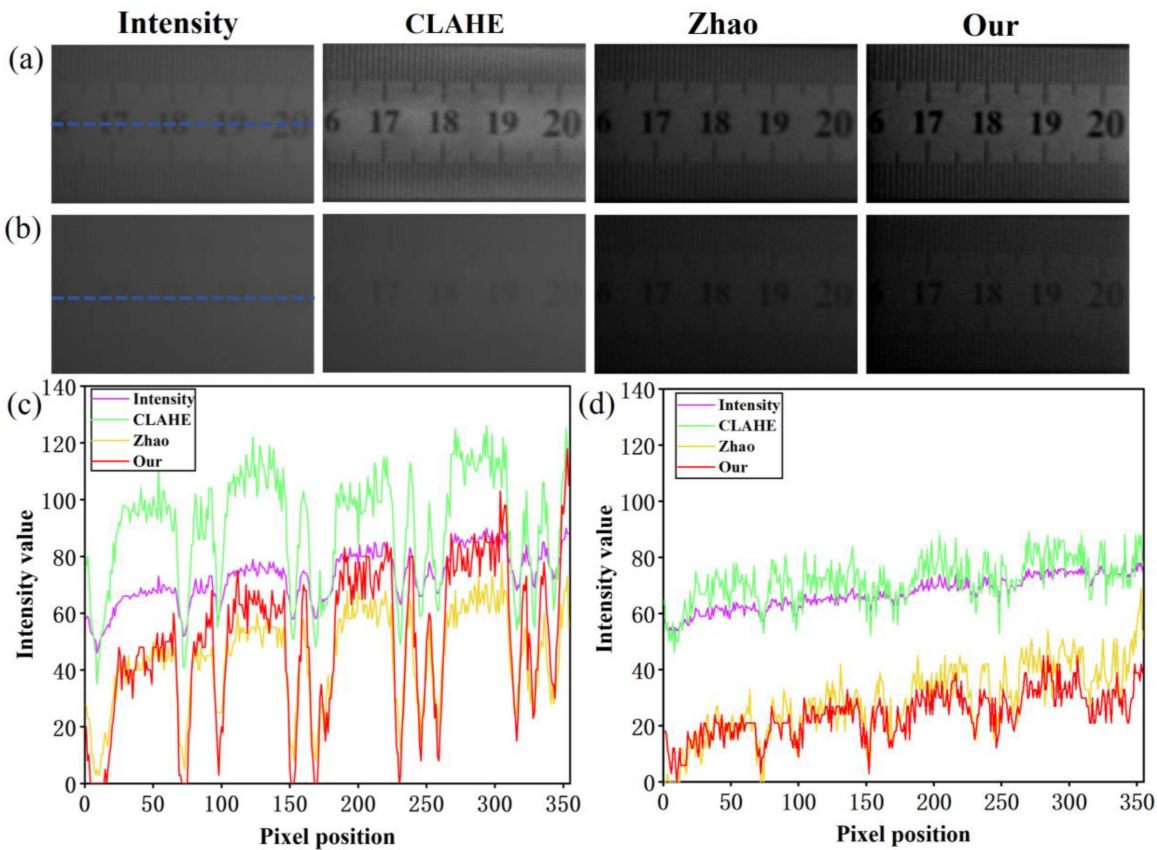

Fig. 9. Recovery results and intensity distribution along the blue dashed line of steel ruler images without background region between the proposed and other methods. (a) The results for milk concentration of 2.466 g/L. (b) The results for milk concentration of 3.695 g/L. (c) Corresponding intensity distribution for milk concentration of 2.466 g/L. (d) Corresponding intensity distribution for milk concentration of 3.695 g/L.

To verify the descattering effect of the proposed method on targets with low DoP, a piece of white fabric with low DoP featuring the letters "CUST" written in black carbon pen is selected as the target. The turbid water environment with milk concentrations of 2.466 g/L and 3.695 g/L are used. Image segmentation is applied to remove the background regions, isolating the target with low DoP. Fig. 10 displays the image of this target in clear water, with its C value in the upper left corner. For comparison, the performance of the method was evaluated against CLAHE and Zhao's method, with the recovered images presented in Fig. 11.
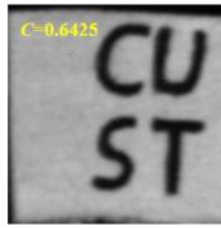
Fig. 10.   Intensity image of the white fabric with the letters "CUST" written on it in clear water.
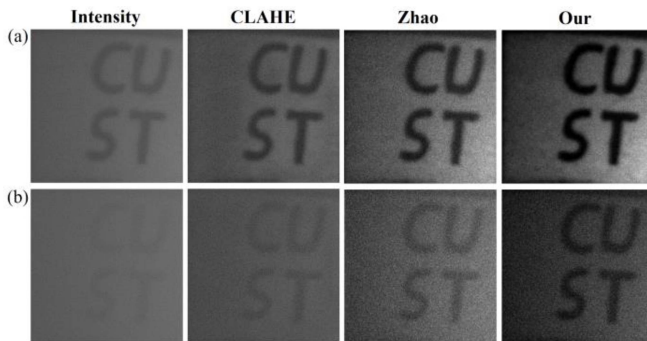

Fig. 11.   Recovery results of white fabric images without background region between the proposed and other methods. (a) The results for milk concentration of 2.466 g/L. (b) The results for milk concentration of 3.695 g/L.

TABLE II
C, SSIM AND EME OF RECOVERED IMAGES BY DIFFERENT METHODS IN FIGS. 9 AND 11

Image	Evaluations	Intensity	CLAHE	Zhao	Our
	C	0.1262	0.1785	0.3313	0.4421
Fig.9(a)	SSIM	0.2469	0.3782	0.4486	0.5698
	EME	0.9180	2.7074	11.028	12.1606
	C	0.0960	0.1062	0.3008	0.4135
Fig. 9(b)	SSIM	0.0914	0.1021	0.1475	0.1724
	EME	0.8635	2.6703	5.2792	8.9835
	C	0.0991	0.1692	0.3967	0.5046
Fig.11(a)	SSIM	0.0998	0.3328	0.4556	0.5341
	EME	0.8911	2.4578	8.8613	9.9155
	C	0.0613	0.0887	0.2451	0.3902
Fig.11(b)	SSIM	0.0268	0.1752	0.4166	0.5066
	EME	0.8342	2.3242	4.6475	6.4432

In the intensity imaging results, the image appeared blurred due to the haze effect caused by the backscattered light. At the milk concentration of 3.695 g/L, the outlines and details of the letters on the white fabric are barely discernible. CLAHE enhanced the image by stretching its gray levels. However, the recovery results are similar to the original intensity image, with limited improvement. The method of Zhao performed well at milk concentrations of 2.466 g/L, but when milk concentrations were 3.695 g/L, its descattering effect was less effective because it only considered a single value of P_B. In contrast, the proposed method eliminates the backscattered light more obviously at both milk concentrations of 2.466 g/L and 3.695 g/L, resulting in clearer and more prominent letter outlines.

The image quality was evaluated using the metrics C, SSIM, and EME, with the results shown in Table II. In the case of low scattering (milk concentration of 2.466 g/L), as shown in Figs. 9(a) and 11(a) in Table II, both the proposed method and Zhao's method perform better on the quantitative metrics, with the proposed method yielding the highest contrast. In the case of high scattering (milk concentration of 3.695 g/L), as shown in Figs. 9(b) and 11(b) in Table II, intensity image evaluation values are significantly reduced. At the same time, the evaluation value of the recovered images by other methods also significantly lower due to errors in the estimation of the backscattering information. Nevertheless, the three-evaluation metrics for the proposed method remain the highest, indicating its superior descattering performance in targets with high or low DoP images without background region.

V. CONCLUSION

This study proposes an underwater polarization imaging method based on DCP estimation of background light. This method effectively removes target interference from the background light calculation, achieving a global and accurate estimation of P_B and B, significantly enhancing the clarity and quality of underwater images. The method eliminates the need for human-machine interaction. It overcomes the limitations of manually selecting background regions in conventional methods, enabling real-time imaging. In addition, it accounts for the polarization characteristics of the target and effectively recovers both highly and weakly polarized targets in scattering media of various concentrations, demonstrating excellent scattering suppression. Both qualitative and quantitative exp-erimental results show that this method can significantly reduce backscattered light, recover detailed image information, and improve visual quality, regardless of the presence of background regions. The proposed method shows great potential in fields such as underwater rescue and environ-mental monitoring. In the current study, only targets with single polarization characteristics are considered in the field of view. Future research will focus on recovering targets with complex polarization characteristics.

REFERENCES

[1] S. Komatsu, A. Markman, and B. Javidi, "Optical sensing and detection in turbid water using multidimensional integral imaging," *Opt. Lett.*, vol. 43, no. 14, pp. 3261–3264, 2018, doi: 10.1364/OL.43.003261.

[2] R. Schettini and S. Corchs, "Underwater image processing: State of the art of restoration and image enhancement methods," *EURASIP J. Adv. Signal Process.*, vol. 2010, pp. 1–14, Dec. 2010, doi: 10.1155/2010/746052.

[3] J. Guan and J. Zhu, "Target detection in turbid medium using polarization-based range-gated technology," *Opt. Exp.*, vol. 21, no. 12, 2013, Art. no. 14152, doi: 10.1364/OE.21.014152.

[4] C. O. Ancuti, C. Ancuti, C. De Vleeschouwer, and P. Bekaert, "Color balance and fusion for underwater image enhancement," *IEEE Trans. Image Process.*, vol. 27, no. 1, pp. 379–393, Jan. 2018, doi: 10.1109/TIP.2017.2759252.

[5] K. He, J. Sun, and X. Tang, "Single image haze removal using dark channel prior," *IEEE Trans. Pattern Anal. Mach. Intell.*, vol. 33, no. 12, pp. 2341–2353, Dec. 2011, doi: 10.1109/TPAMI.2010.168.

[6] A. M. Reza, "Realization of the contrast limited adaptive histogram equalization (CLAHE) for real-time image enhancement," *VLSI Signal Process.*, vol. 1, no. 38, pp. 35–44, 2004.

[7] M. Zheng and W. Luo, "Underwater image enhancement using improved CNN based defogging," *Electronics*, vol. 11, no. 1, p. 150, 2022, doi: 10.3390/electronics11010150.

[8] J. Lu, N. Li, S. Zhang, Z. Yu, H. Zheng, and B. Zheng, "Multi-scale adversarial network for underwater image restoration," *Opt. Laser Technol.*, vol. 110, pp. 105–113, 2019, doi: 10.1016/j.optlastec.2018.05.048.

[9] H. Hu, Y. Zhang, X. Li, Y. Lin, Z. Cheng, and T. Liu, "Polarimetric underwater image recovery via deep learning," *Opt. Lasers Eng.*, vol. 133, 2020, Art. no. 106152, doi: 10.1016/j.optlaseng.2020.106152.

[10] Y. Y. Schechner and N. Karpel, "Recovery of underwater visibility and structure by polarization analysis," *IEEE J. Ocean. Eng.*, vol. 30, no. 3, pp. 570–587, Jul. 2005, doi: 10.1109/JOE.2005.850871.

[11] B. Huang, T. Liu, H. Hu, J. Han, and M. Yu, "Underwater image recovery considering polarization effects of objects," *Opt. Exp.*, vol. 24, no. 9, pp. 9826–9838, 2016, doi: 10.1364/OE.24.009826.

[12] K. O. Amer, M. Elbouz, A. Alfalou, C. Brosseau, and J. Hajjami, "Enhancing underwater optical imaging by using a low-pass polarization filter," *Opt. Exp.*, vol. 27, no. 2, pp. 621–643, 2019, doi: 10.1364/OE.27.000621.

[13] P. Qi et al., "U2R-pGAN: Unpaired underwater-image recovery with polarimetric generative adversarial network," *Opt. Lasers Eng.*, vol. 157, Oct. 2022, Art. no. 107112, doi: 10.1016/j.optlaseng.2022.107112.

[14] T. Treibitz and Y. Y. Schechner, "Active polarization descattering," *IEEE Trans. Pattern Anal. Mach. Intell.*, vol. 31, no. 3, pp. 385–399, Mar. 2009, doi: 10.1109/TPAMI.2008.85.

[15] M. Dubreuil, P. Delrot, I. Leonard, A. Alfalou, C. Brosseau, and A. Dogariu, "Exploring underwater target detection by imaging polarimetry and correlation techniques," *Appl. Opt.*, vol. 52, no. 5, pp. 997–1005, 2013, doi: 10.1364/AO.52.000997.

[16] Y. Zhao, W. He, H. Ren, Y. Li, and Y. Fu, "Polarization descattering imaging through turbid water without prior knowledge," *Opt. Lasers Eng.*, vol. 148, 2022, Art. no. 106777, doi: 10.1016/j.optlaseng.2021.106777.

[17] H. Hu, L. Zhao, X. Li, H. Wang, and T. Liu, "Underwater image recovery under the nonuniform optical field based on polarimetric imaging," *IEEE Photon. J.*, vol. 10, no. 1, Feb. 2018, Art. no. 6900309, doi: 10.1109/JPHOT.2018.2791517.

[18] H. Wang et al., "Automatic underwater polarization imaging without background region or any prior," *Opt. Exp.*, vol. 29, no. 20, pp. 31283–31295, 2021, doi: 10.1364/OE.434398.

[19] P. Han, F. Liu, Y. Wei, and X. Shao, "Optical correlation assists to enhance underwater polarization imaging performance," *Opt. Lasers Eng.*, vol. 134, 2020, Art. no. 106256, doi: 10.1016/j.optlaseng.2020.106256.

[20] S. Yang, B. Qu, G. Liu, D. Deng, S. Liu, and X. Chen, "Unsupervised learning polarimetric underwater image recovery under nonuniform optical fields," *Appl. Opt.*, vol. 60, no. 26, pp. 8198–8205, 2021, doi: 10.1364/AO.432994.

[21] T. Li, J. Wang, and K. Yao, "Visibility enhancement of underwater images based on active polarized illumination and average filtering technology," *Alexandria Eng. J.*, vol. 61, no. 1, pp. 701–708, Jan. 2022, doi: 10.1016/j.aej.2021.06.007.

[22] Y. Wei, P. Han, F. Liu, and X. Shao, "Enhancement of underwater vision by fully exploiting the polarization information from the stokes vector," *Opt. Exp.*, vol. 29, no. 14, pp. 22275–22287, 2021, doi: 10.1364/OE.433072.

[23] J. Deng, J. Zhu, H. Li, X. Zhang, F. Guo, and X. Hou, "Real-time underwater polarization imaging without relying on background," *Opt. Lasers Eng.*, vol. 169, Oct. 2023, Art. no. 107721, doi: 10.1016/j.optlaseng.2023.107721.

[24] P. Drews, E. Nascimento, F. Moraes, S. Botelho, and M. Campos, "Transmission estimation in underwater single images," in *Proc. IEEE Int. Conf. Comput. Vis. Workshops*, 2013, pp. 825–830, doi: 10.1109/IC-CVW.2013.113.

[25] J. Guan, M. Ma, and Y. Huo, "Underwater polarimetric dark channel prior descattering," *Opt. Laser Technol.*, vol. 175, Aug. 2024, Art. no. 110864, doi: 10.1016/j.optlastec.2024.110864.

[26] W. Feng, G. Wu, Y. Wu, Y. Miao, and B. Liu, "Algorithm for underwater polarization imaging based on global estimation," *Acta Optica Sinica*, vol. 40, no. 21, pp. 75–83, 2020.

[27] F. Liu et al., "Deeply seeing through highly turbid water by active polarization imaging," *Opt. Lett.*, vol. 43, no. 20, pp. 4903–4906, 2018, doi: 10.1364/OL.43.004903.

[28] C. Gao et al., "Underwater polarization de-scattering imaging based on orthogonal polarization decomposition with low-pass filtering," *Opt. Lasers Eng.*, vol. 170, 2023, Art. no. 107796, doi: 10.1016/j.optlaseng.2023.107796.

[29] M. Shan et al., "Global optimal reconstruction of underwater polarization imaging using low-pass frequency-filtering constraint," *Opt. Lasers Eng.*, vol. 181, 2024, Art. no. 108414, doi: 10.1016/j.optlaseng.2024.108414.

[30] D. Risovic, "Effect of suspended particulate-size distribution on the backscattering ratio in the remote sensing of seawater," *Appl. Opt.*, vol. 41, no. 33, pp. 7092–7101, 2002, doi: 10.1364/ao.41.007092.

[31] D. Risovic, "Two-component model of sea particle size distribution," *Deep-Sea Res. Part I, Oceanographic Res. Papers*, vol. 40, no. 7, pp. 1459–1473, 1993, doi: 10.1016/0967-0637(93)90123-K.

[32] Y. Piederriere, F. Boulvert, J. Cariou, B. Le Jeune, Y. Guern, and G. Le Brun, "Backscattered speckle size as a function of polarization: Influence of particle-size and -concentration," *Opt. Exp.*, vol. 13, no. 13, pp. 5030–5039, 2005, doi: 10.1364/opex.13.005030.

[33] Z. Wang, A. C. Bovik, H. R. Sheikh, and E. P. Simoncelli, "Image quality assessment: From error visibility to structural similarity," *IEEE Trans. Image Process.*, vol. 13, no. 4, pp. 600–612, Apr. 2004, doi: 10.1109/tip.2003.819861.